Topology-Aware Quantum Graph Neural Networks for Sum-Rate Maximization in Fluid Antenna Systems

Okzata Recy, *Student Member, IEEE,* Bhaskara Narottama, *Member, IEEE,* and Trung Q. Duong, *Fellow, IEEE*

***Abstract*—This paper presents a quantum graph-based solution that leverages a quantum circuit to improve learning efficiency, towards maximizing the sum-rate of wireless communication with fluid antennas in dynamic environments. The employed quantum graph neural networks (QGNN) consists of three main blocks, including (i) a quantum encoding layer, (ii) a quantum graph neural network layer, and (iii) an optimizer layer, which collectively comprise the end-to-end learning workflow. The QGNN adjusts parameters through a quantum graph neural network layer, utilizing basic linear gates on a parameterized quantum circuit (PQC) platform. Additionally, the QGNN circuit is designed with shallow depth and optimized gate composition to reduce quantum resource usage and accelerate convergence during training. The results demonstrate that the proposed QGNN offers competitive performance relative to the existing PQC model. Furthermore, this paper highlights the versatility of quantum graph-based solutions for addressing dynamic, topology-aware wireless network problems.**

***Index Terms*—Fluid antenna systems; quantum graph neural networks; quantum machine learning.**

I. Background

MULTIPLE-input multiple-output (MIMO) antenna systems have been widely adopted in wireless communication networks, exploiting spatial diversity by using multiple antennas at both the base station (BS) and user sides. However, the continual growth in MIMO antenna elements leads to larger arrays, encumbering user equipment (UE) in size. This has driven a shift from fixed antenna configurations to reconfigurable designs, with many studies proposing flexible structures, such as fluid-based or pixelated metal elements, collectively referred to as fluid antenna systems (FAS) [1]. Conceptually, FAS is not restricted to a specific material, as it can be realized using liquid, reconfigurable pixels, or any technique enabling movable antenna elements. Irrespective of the implementation medium, FAS can be viewed as a holographic MIMO system with antenna selection, wherein each port precisely samples a spatial point across a continuous electromagnetic field. In this context, the channel reconstruction resembles that of a band-limited field, which theoretically requires only half-wavelength sampling for perfect recovery. FAS dynamically selects antenna ports, i.e., the spatial positions, with the strongest received signals, facilitating spatial diversity gains without the excessive physical footprint typical of conventional antennas. In this context, the joint optimization of port selection and beamforming to maximize achieved rates has been addressed in [2] and [3]. Along similar lines, [4] employs convex relaxation techniques to approximate the channel capacity through a joint transmit and receive antenna port selection scheme for fluid-MIMO systems. Several studies also investigate learning-based data-driven approaches for FAS optimization, including the study in [5], which considers bandit learning to optimize antenna port selection under time-varying channel state information (CSI); and [6], which utilizes a deep learning approach for channel extrapolation from incomplete CSI data. However, none of these studies adopts graph-based learning.

Many wireless networks and systems inherently align with graph-based representation and exhibit non-Euclidean structures, which are reflected in the FAS communication links between BS antennas and UE ports. Hence, graph-based modeling is better suited to capture irregular topologies than grid-based structures. Graph neural networks (GNN) have been widely adopted to model these topologies by representing the relationships among vertices and edges. In particular, classical GNNs have been applied to such applications with promising results [7]. Additionally, quantum learning models provide expressive representations within high-dimensional Hilbert spaces, even when utilizing a small number of quantum bits. Quantum GNN (QGNN) offers a complementary approach by exploiting quantum properties, such as parallelism and entanglement, to enhance the modeling of graph-structured wireless systems. These considerations motivate the exploration of graph-based representations of wireless networks integrated with a quantum learning model [8]. Despite its potential, a noticeable gap exists in the adoption of quantum graph-based learning for future wireless systems, particularly FAS.

The contributions of this paper are outlined in the following.

- This study leverages graph-based representations of wireless systems to facilitate quantum graph-based learning. In these graphs, vertices denote transmitter–receiver pairs, while edges capture their mutual interactions, such as channel information. By combining quantum computing with learning approaches, the graphical representations of wireless systems can be transformed into a unified topology that incorporates different quantum operations. This graph representation captures the spatial dependencies and dynamic behavior of wireless networks. By mapping

The authors are with the Faculty of Engineering and Applied Science, Memorial University, St. John's, NL A1B 3X5, Canada (e-mail: {orecy, bnarottama, tduong}@mun.ca). This work was supported by the Canada Excellence Research Chair (CERC) Program CERC-2022-00109, by the Natural Sciences and Engineering Research Council of Canada (NSERC) Discovery Grant Program RGPIN-2025-04941, and by the NSERC CREATE program (Grant number 596205-2025).

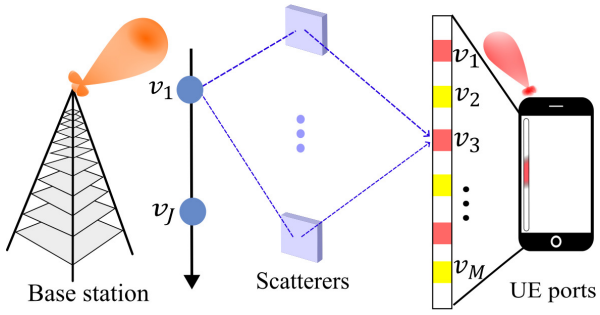

Fig. 1: Wireless communication environment entailing fluid antenna systems.

the irregular and time-varying wireless environment into the graph domain, we establish a learning solution that supports the optimization of wireless systems operating over graph-based structures, such as in FAS. To the best of the authors' knowledge, this is the first study that designs a QGNN-based optimization solution tailored to the topology of the wireless system at hand. In comparison, while some studies leverage quantum learning models for optimization and prediction, they typically do not account for the graph-based structure inherent in wireless systems.

- This study demonstrates the adoption of the proposed QGNN for wireless communication, particularly in FAS. Numerical results are presented to evaluate the QGNN-based learning solution, with the objective of optimizing UE antenna port selection to maximize the sum rate. The proposed QGNN model is shown to be feasible for practical implementation in FAS.
- This study presents a quantum operation of low complexity that represents a graph vertex with a reduced number of gates and qubits, facilitating implementation on early-stage quantum processors. As an illustrative example, we use the proposed QGNN solution to maximize the UE rate in FAS, through optimizing both the antenna port positioning and transmit precoding. The numerical results are analyzed to investigate the performance of the proposed solution.

Notations. We use bold uppercase and lowercase letters (e.g. $\mathbf{H}, \mathbf{v}$) to represent matrices and vectors, respectively. The set of integers, the set of complex numbers, the real part, and the imaginary part are conveyed by $\mathbb{Z}$, $\mathbb{C}$, $\mathfrak{Re}(\cdot)$, $\mathfrak{Im}(\cdot)$, respectively. The transpose and Hermitian operations are defined by $[\cdot]^T$ and $[\cdot]^H$, respectively. Quantum gates are denoted by symbols such as $\mathsf{R}_z(\theta)$, which refers to a rotation around the z-axis by an angle θ. $\mathsf{U}^{\otimes\mathcal{E}}$ indicates that the unitary gate U is applied in parallel to $\mathcal{E}$ qubits.

II. System Model

We study a wireless downlink scenario where a BS with J fixed antenna positions communicates with a UE equipped with M FA ports, as illustrated in Fig. 1. We focus on optimizing the UE's fluid antenna by dynamically activating selected ports in response to pertinent variables such as CSI. The channel is assumed to operate in a scattering channel environment with multipath propagation, modeled using a scatter-based geometric approach as in [2]. The overall complex channel matrix is represented as $\mathbf{H} = \mathbf{B}^H\mathbf{O}\mathbf{A} \in \mathbb{C}^{M\times J}$, where $\mathbf{A}$ and $\mathbf{B}$ denote the field response matrices of transmit and receive arrays, respectively, and $\mathbf{O}$ is an i.i.d. complex Gaussian random variable, such that $\mathbb{C}\mathcal{N}(\mu, \sigma^2)$. Our objective is to maximize the UE's achieved rate, which can be computed by summing the achieved rate based on the selected ports, as

$$R = \sum_{m=1}^{M} \log_2\left(1 + \frac{\Gamma|\mathbf{h}_m^H \mathbf{p}_m \mathbf{v}_m|^2}{\sigma_m^2}\right), \tag{1}$$

where $\mathbf{v}$ and $\mathbf{p}$ denote the transmit precoding and port selection vectors, respectively. The BS transmit power Γ is assumed to be uniformly allocated across the BS antennas. To this aim, we first optimize the BS's transmit precoding vector, followed by identifying the port $p^* \in \{1, 2, \cdots, P\}$ that maximizes the achieved rate at the fluid antenna-equipped UE. We aim to maximize the UE sum rate as follows:

$$\underset{\mathbf{v},\,\mathbf{p}}{\text{maximize}} \quad R(\mathbf{v}, \mathbf{p}) \tag{2a}$$

$$\text{subject to} \quad p_m \in \{1, 2, \cdots, P\}, \forall p_m \in \mathbf{p}, \tag{2b}$$

$$|v_j|^2 \leq 1, \forall v_j \in \mathbf{v}, \tag{2c}$$

where $R(\mathbf{v}, \mathbf{p})$ denotes the UE achieved rate, defined by the transmit precoding vector $\mathbf{v}$ and the port selection vector $\mathbf{p}$, $\mathbf{p} = [p_1, \cdots, p_M]^T \in \mathbb{Z}^{M\times 1}$. $\mathbf{v}_j$ and $\mathbf{p}_m$ correspond to the j-th entry of the transmit precoding vector and the m-th selected port, respectively, with $j \in \{1, 2, \cdots, J\}$ and $m \in \{1, 2, \cdots, M\}$. The UE ports are sequenced by integer indices in ascending order, as in $p_1 < p_2 < \cdots < p_M$. As per (2b), each selected port index p_m must be a discrete integer within the range $\{1, 2, \cdots, P\}$. This constraint is satisfied by selecting the port index that maximizes the achieved rate at the m-th port based on the quantum decoding output, thereby ensuring a valid mapping between the transmit precoding entries and the UE ports. To maintain the power budget of each element port, each entry of the precoding vector $\mathbf{v}$ shall satisfy (2c), regardless of the phase contribution. The problem in (2) is non-trivial because it requires joint optimization at both the UE and BS sides. In addition, the problem becomes increasingly challenging as the network topology scales, particularly with the growth in the number of antennas/ports at both BS and UE. Similarly, the study of [9], which optimizes both the transmit waveform and receive filtering, took a similar route, using a deep learning approach.

III. Adopting QGNNs

As shown in Fig. 2(a), the QGNN architecture comprises three major components: (i) a quantum encoding layer that initializes quantum states representing the input graph features and topology, such as connectivity between BS and UE ports, (ii) a quantum graph neural network layer, the core of graph-based quantum learning, that propagates and aggregates information across graph structures using parameterized quantum circuits (PQCs), and (iii) a network optimization

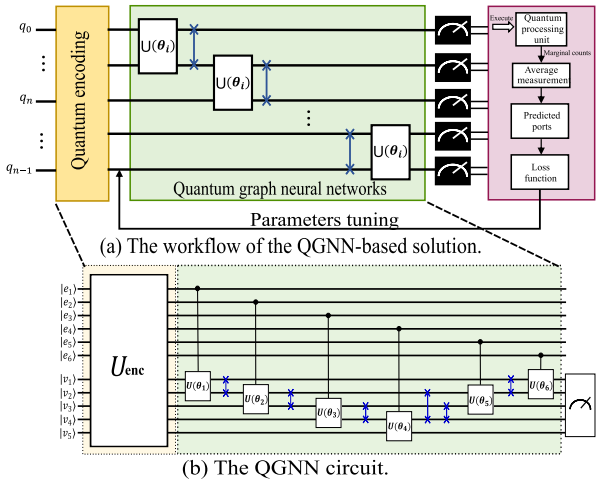

(a) The workflow of the QGNN-based solution.

(b) The QGNN circuit.

Fig. 2: The proposed quantum-based graph.

process, that receives classical values obtained from quantum measurements. These values are subsequently fed into a classical optimizer, which updates the tunable parameters of the PQCs, enabling a closed-loop parameter training process within a quantum-enabled learning workflow. To begin with, classical graph data are first transformed into a quantum-based graph representation $\mathcal{G}_q = (\mathcal{V}_q, \mathcal{A})$, each vertex i is represented by a quantum state $|v_i\rangle$, constituting the vertex set $\mathcal{V}_q = \{|v_1\rangle, |v_2\rangle, \cdots, |v_N\rangle\}$, and

$$\mathcal{A} = \begin{bmatrix} 0 & 0 & e_1 & e_2 & e_3 \\ 0 & 0 & e_4 & e_5 & e_6 \\ e_1 & e_4 & 0 & 0 & 0 \\ e_2 & e_5 & 0 & 0 & 0 \\ e_3 & e_6 & 0 & 0 & 0 \end{bmatrix} \tag{3}$$

is the adjacency matrix capturing the topology.

Quantum graph neural layer. Following quantum encoding and state preparation, the controlled-unitary custom parameterized gate $\mathsf{U}(\theta_n)$ is then applied. We design $\mathsf{U}(\theta_n)$ as a shallow-depth sequence of available basic gates, consisting of only two C_z gates and a single-qubit parameterized rotation gate. Multiple instances of $\mathsf{U}(\theta_n)$ are applied to each quantum state according to the adjacency matrix $\mathcal{A}$ in (3), constructing a fully interconnected communication graph topology, wherein each pair of quantum states shall interact via a single $\mathsf{U}(\theta_n)$. As a concrete example, the quantum circuit in Fig. 2(b) constructs a graph with five vertices connected to each other through weighted edges, representing a particular communication scenario. In this circuit, $M \times J$ qubits $|e\rangle$ are used to encode the adjacency matrix, while $M + J$ qubits $|v\rangle$ are allocated to encode the feature vectors of the vertices. Additionally, six identical controlled-unitary gates establish the connections between the BS antennas and UE ports. When interactions between non-adjacent qubits are necessary, "swap" gates are inserted between $\mathsf{U}(\theta_n)$ operations.[1] These gates are crucial to preserve the structural alignment between the graph and the underlying communication model, ensuring that message-passing operations within the circuit accurately reflect the link-level connectivity between wireless system/network elements. At the end of the quantum circuit, a projective measurement is performed. The resulting measurement outcomes from the QGNN decoder are translated into the optimization variables, the transmit precoding vector $\mathbf{v}$, and the port selection vector $\mathbf{p}$. In this paper, the quantum observable $\mathbb{M}$ measures the BS's qubits of the vertex representation, extracting phase-related values that correspond to $\mathbf{v}$. The port selection is decided based on the QGNN decoder, resulting in an achieved rate, computed as $p = \arg\max_i \text{SNR}_i(\mathbf{v})$, in which $\mathbf{v}$ is the transmit precoding vector derived from the measurement outcomes. The expectation value pertinent to measuring $\mathbb{M}$ can be expressed as $\text{Tr}\left(\mathbb{M} \cdot \mathsf{U}_{\text{graph}} \cdot |\psi_{\text{enc}}\rangle \langle\psi_{\text{enc}}| \mathsf{U}_{\text{graph}}^{\dagger}\right)$, where $\text{Tr}(\cdot)$ denotes the trace operation, $\mathsf{U}_{\text{graph}}$ is the unitary operator representing the full graph structure, and $|\psi_{\text{enc}}\rangle = \mathsf{U}_{\text{enc}} \cdot |0\rangle^{\otimes N_{\text{qub}}}$ denotes the input state prepared by encoding the classical graph features, with N_{qub} denotes the total number of qubits within the QGNN circuit. The measurement observable is defined as $\mathbb{M} = \sigma_U^{\otimes 2} \otimes \sigma_0^{\otimes(N_{\text{qub}}-2)}$, where $\sigma_U = |1\rangle\langle 1|$ and $\sigma_0 = |0\rangle\langle 0| + |1\rangle\langle 1|$ are the projective and identity operators, respectively. In this paper, we adopt an unsupervised learning principle, where the loss function with respect to the i-th parameter at iteration t, $\mathcal{L}\left(\theta_i^{(t)}, \mathbf{v}, \mathbf{p}; \mathbf{H}^{(t)}\right)$ is defined as the negative of the achieved performance metric. In the considered scenario, the focus is on the UE with limited mobility, where the channel variations are relatively slow. This assumption allows the model to remain effective without requiring reinforcement learning-based adaptation.

Network optimization process. Since the optimization problem in (2) is non-concave and involves coupled variables $\mathbf{v}$ and $\mathbf{p}$, it is remarkably challenging to trace its direct solutions. This paper represents an initial effort in applying learning-based optimization to fluid antenna systems and aims to enhance efficiency through data-driven design [10]. Studies in [11], [12] employ unfolding learning strategies, which decompose a problem into subproblems, as a classical approach to accelerate the learning process. In a similar manner, we partition the optimization problem into two subproblems and address them separately through learning-based methods in two distinct optimization stages.

1) *BS's transmit precoding optimization:* To start with, we assume that UE ports are fixed in positions, allowing us to focus solely on optimizing the transmit precoding vector. This relaxation simplifies the problem in (2) to the following subproblem:

$$\underset{\mathbf{v}}{\text{maximize}} \quad R(\mathbf{v} \mid p_m) \tag{4a}$$

$$\text{subject to} \quad |v_j|^2 \leq 1, \forall v_j \in \mathbf{v}. \tag{4b}$$

2) *UE ports selection:* We then assume a fixed transmit precoding vector, directing the optimization towards maximizing the total transmission rate across all ports, reducing (2) to the

[1]Each of which *swaps* qubits as if "moving" them into physical proximity without disrupting the relationships of other qubits. In many cases, physically moving qubits is not feasible. For which reason, "swap" gates are employed instead to logically reposition quantum information without physically altering the hardware.

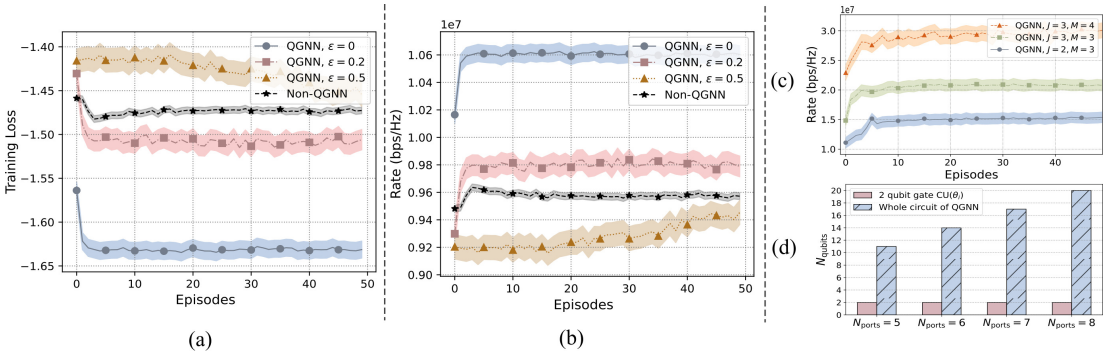

Fig. 3: The QGNN performance, including: (a) training loss behavior, (b) the achieved rate during the training episodes, and (c) the achieved rate under different BS-UE ports configurations, along with (d) qubit requirements as the topology grows.

following subproblem:

$$\underset{p}{\text{maximize}} \quad R(\mathbf{p}) \tag{5a}$$

$$\text{subject to} \quad p_m \in \{1, 2, \cdots, P\}, \forall p_m \in \mathbf{p}. \tag{5b}$$

The achieved rate $R(\mathbf{p})$ in (5) is computed based on the SNR observed at the selected port. The port indices are obtained from the set of values produced by the QGNN decoder. Based on these outputs, a mapping function selects the candidate UE ports from the available port set. This results in port-selection vector $\mathbf{p} = [p_1, \cdots, p_m]^T \in \mathbb{Z}_+^{(M-1)\times 1}$, which specifies the chosen UE ports, where each $p_m \in \mathbb{Z}_+$ denotes the integer index of a selected port, ordered such that $p_1 < \cdots < p_m$, in accordance with the constraint in (5b). Subsequently, a normalized phase vector $\mathbf{v}_m = \frac{\exp(j\theta_m)}{|\exp(j\theta_m)|}$ is obtained from the QGNN decoder, resulting in the effective channel matrix $\mathbf{H}_{\text{pref}} = \mathbf{B}(\mathbf{p})^H$. Given a precoding vector and channel realization, the SNR at port m is given by $\zeta_m = \frac{|\mathbf{b}(p_m)^H \mathbf{v}_i|^2}{\sigma^2}, \forall m$. It is important to note that the proposed approach accommodates larger numbers of ports, with the number of required qubits increasing proportionally to the size of the network elements.

IV. Numerical Results

This section presents the numerical results to validate the advantage of the proposed QGNN applied to the FAS network system model. During the training, we assume that the BS is equipped with two antennas, while the UE is configured with three available ports. Both the BS antennas and UE ports spacings are set to $\lambda/2$. The channel includes two transmit κ_t and two receive κ_r paths, and the channel bandwidth is assumed to be 6.5 MHz. To obtain the loss gradient, the parameter shift rule is then applied during training of the QGNN. We evaluate the proposed solution under imperfect channel conditions induced by quantum noise. The imperfection is modeled using Pauli-X errors with probabilities $\epsilon = \{0, 0.2, 0.5\}$ applied to the proposed QGNN-based solution. Here, ϵ represents the probability that quantum noise occurs in quantum hardware. For example, $\epsilon = 0.2$ indicates a 20 % chance that noise affects the system. Moreover, these simulations are carried out on the IBM quantum platform using Qiskit. For comparison, we include a generalized PQC model and adjust its gate count so that both approaches operate under comparable quantum resource constraints. This model serves as a fitting benchmark owing to its demonstrated success in quantum-enabled wireless optimization and beyond [13]. Further details on this quantum model are provided in Appendix A.[2] Fig. 3(a) shows the corresponding training loss evolution of the proposed QGNN and a conventional learning model (termed "Non-QGNN") over 50 training episodes. Both models displayed a decreasing loss trend over the training period. We can observe that: (i) the QGNN without noise ($\epsilon = 0$) achieves the lowest training loss, and shows a notably steeper decline in the early episodes, indicating fast convergence toward a stable solution. Around the second episode, it rapidly converges to its best possible training outcomes, while (ii) the QGNN with $\epsilon = 0.5$ suffers in finding the solution due to the frequent noise, (iii) the QGNN with $\epsilon = 0.2$ converges effectively as well, but to slightly higher loss than the noiseless case. However, it still outperforms the Non-QGNN baseline. This highlights both the robustness of QGNN under moderate noise and its benefits over Non-QGNN approaches. By encoding the wireless network's graph-based connectivity, it acquires better comprehension of the network structure, leading to both fast convergence and diminished training loss. By comparison, the Non-QGNN model relies on channel coefficients alone as input features, neglecting topological context, resulting in sluggish convergence and curtailed learning performance.

In a similar manner, Fig. 3(b) shows the evolution of the achieved sum rate for different QGNN noise levels and the Non-QGNN baseline throughout the training process. As observed, the proposed solution, QGNN with $\epsilon = 0$, converged to a higher and more stable communication rate within the first few episodes, showing minimal variance. This exhibits its robustness and consistent learning progression. When noise is introduced ($\epsilon = 0.2$), the QGNN still converges effectively and consistently outperforms the Non-QGNN. In contrast thereto, the Non-QGNN displayed a noticeable fluctuating trend, with the achieved rate undergoing significant oscillation across episodes. Despite an initial increase, the rate eventually

[2]To maintain a fair comparison, the number of tunable parameters and quantum gates was set to be equal to the proposed QGNN.

saturated at a lower level compared to the QGNN. However, as expected, under strong noise conditions, the QGNN exhibits higher fluctuations and saturates the lowest achieved rate among all cases.

Furthermore, we next examine how the proposed QGNN behaves when the wireless topology grows. The observation is obtained by increasing the number of BS antennas J and the UE ports M, which focuses on the noiseless case to isolate the QGNN model's impact. As shown in Fig. 3(c), all configurations with higher antennas and ports consistently exhibit an improvement in the achieved rate due to the expanded spatial degrees of freedom and larger port-selection space. This trend, in particular, confirms that QGNN effectively leverages the addition of antenna–port combinations to identify port and precoder pairs that align more favorably with the effective channel. Regarding the quantum circuit, the number of qubits in the quantum circuit reflects the full topology of the wireless graph and increases accordingly as the network grows. The total qubit count follows $N_{\text{qub}} = (M \times J) + (M + J)$, where M and J denote the number of available UE ports and BS antennas, respectively, with the scaling shown in Fig. 3(d). These results underline the benefits of QGNN in noiseless and moderately noisy environments, but emphasize the need for noise-mitigation designs to maintain overall performance under stronger noise conditions.

V. Conclusion and Further Exploration

This paper presents a QGNN-based learning solution for representing and optimizing wireless networks, with a particular focus on fluid antenna systems. By encoding channel information into the quantum circuit and performing graph-based message passing, the proposed QGNN model facilitates a structured representation of the wireless network, enabling quantum-driven learning and optimization. The results serve as empirical validation of the proposed QGNN model, as reflected by a consistent reduction in loss and improvements in achieved sum rate, particularly around the 2^{nd} training episode. Such findings suggest the capability of quantum models to effectively capture relational structures between wireless network variables, even with a minimal quantum circuit depth, in accordance with the studies such as [14]. This study provides an important step toward applying quantum learning to graph-based wireless networks, albeit with the performance evaluated upon the simulation results, assuming an ideal quantum computing environment. Facilitated by recent developments in quantum circuit architectures (e.g., [15]), future exploration may include adjustable circuits to enable adaptive reinforcement learning in high mobility scenarios, including uncrewed aerial vehicle-to-everything (UAV-V2X) communications.

Appendix A
A PQC Model for Benchmarking

The quantum-based learning model for benchmarking follows a typical VQC architecture, without any graph-based embeddings integrated into the quantum circuit (for a visual reference, the common architecture can be found in [13, Fig. 4(B)]). To provide a fair comparison, the benchmark model mirrors the quantum state preparation of the proposed QGNN. Each complex channel coefficient is transformed into a quantum state via angle encoding, featuring a combination of gates R_y and R_z, independently applied onto six qubits. The resulting states are then passed through a VQC, composed of a double layer of entangled $\mathsf{C}z$ followed by a single parameterized layer (e.g., an R_y gate), with the number of gates matching that of the proposed QGNN. Afterward, X gates are applied to all qubits to flip their states, enabling the activation of controlled operations. Subsequently, C_x gates are used to entangle the output corresponding to the BS. The first two qubits are then measured using the quantum observable $\mathbb{M}$. Loss gradients are computed using the parameter shift-rule, with each evaluation assuming $N_{\text{shots}} = 1024$, consistent with the QGNN setup.

References

[1] W. Lyu, S. Yang, Y. Xiu, Z. Zhang, C. Assi, and C. Yuen, "Movable antenna enabled integrated sensing and communication," *IEEE Trans. Wireless Commun.*, vol. 24, no. 4, pp. 2862–2875, Jan. 2025.

[2] Y. Chen, M. Chen, H. Xu, Z. Yang, K.-K. Wong, and Z. Zhang, "Joint beamforming and antenna design for near-field fluid antenna system," *IEEE Wireless Commun. Lett.*, vol. 14, no. 2, pp. 415–419, Nov. 2024.

[3] S. Yang, W. Lyu, B. Ning, Z. Zhang, and C. Yuen, "Flexible precoding for multi-user movable antenna communications," *IEEE Wireless Commun. Lett.*, vol. 13, no. 5, pp. 1404–1408, Mar. 2024.

[4] C. N. Efrem and I. Krikidis, "Transmit and receive antenna port selection for channel capacity maximization in Fluid-MIMO systems," *IEEE Wireless Commun. Lett.*, vol. 13, no. 11, pp. 3202–3206, Sep. 2024.

[5] J. Zou, S. Sun, and C. Wang, "Online learning-induced port selection for fluid antenna in dynamic channel environment," *IEEE Wireless Commun. Lett.*, vol. 13, no. 2, pp. 313–317, Oct. 2023.

[6] X. Wu, H. Zhang, C.-C. Wang, and Z. Li, "Channel state information extrapolation in fluid antenna systems based on masked language model," in *Proc. 2024 IEEE Int. Conf. Commun. Workshops (ICC Workshops)*, Jun. 2024, pp. 1383–1388.

[7] T. Chen *et al.*, "A GNN-based supervised learning framework for resource allocation in wireless IoT networks," *IEEE Internet Things J.*, vol. 9, no. 3, pp. 1712–1724, Jun. 2021.

[8] S. Zhang, T. Qiu, N. Chen, H. Ning, M. Han, and X. Liu, "A robust networking model with quantum evolution for Internet of Things," *IEEE Network*, vol. 38, no. 2, pp. 218–224, May 2023.

[9] J. Zhang, Y. Zhu, N. Zhao, S. Jin, X. Wang, D. W. K. Ng, and N. Al-Dhahir, "Deep unfolding learning aided ISAC transceiver design," *IEEE Trans. Wireless Commun.*, vol. 24, no. 10, pp. 8681–8695, May. 2025.

[10] X. Xu, X. Mu, Y. Liu, and A. Nallanathan, "Joint transmit and pinching beamforming for pinching antenna systems (PASS): Optimization-based or learning-based," 2025, doi: 10.48550/arXiv.2502.08637.

[11] B. Feng, C. Feng, K.-K. Wong, and T. Q. Quek, "Deep unfolding neural networks for fluid antenna-enhanced vehicular communication," *IEEE Trans. Veh. Technol.*, vol. 74, no. 9, pp. 14 793–14 798, Apr. 2025.

[12] A. Chowdhury, G. Verma, C. Rao, A. Swami, and S. Segarra, "Unfolding WMMSE using graph neural networks for efficient power allocation," *IEEE Trans. Wireless Commun.*, vol. 20, no. 9, pp. 6004–6017, Apr. 2021.

[13] J. Li *et al.*, "A novel spatial-temporal variational quantum circuit to enable deep learning on NISQ devices," in *Proc. 2023 IEEE Int. Conf. on Quantum Comput. and Eng.*, vol. 1, Sep. 2023, pp. 272–282.

[14] B. Yang *et al.*, "Testing scalable Bell inequalities for quantum graph states on IBM quantum devices," *IEEE J. Emerg. Sel. Top. Circuits Syst.*, vol. 12, no. 3, pp. 638–647, Aug. 2022.

[15] Y. Du, T. Huang, S. You, M.-H. Hsieh, and D. Tao, "Quantum circuit architecture search for variational quantum algorithms," *npj Quantum Info.*, vol. 8, no. 1, p. 62, Apr. 2022.